Retrieval of experimental differential electron–ion elastic scattering cross sections from high-energy ATI spectra of rare gas atoms by infrared lasers

Toru Morishita[1,2]**, Misaki Okunishi**[3]**, Kozo Shimada**[3]**, Georg Prümper**[3]**, Zhangjin Chen**[4]**, Shinichi Watanabe**[1]**, Kiyoshi Ueda**[3] **and C D Lin**[4]

[1] Department of Applied Physics and Chemistry, University of Electro-Communications,
1-5-1 Chofu-ga-oka, Chofu-shi, Tokyo 182-8585, Japan
[2] PRESTO, Japan Science and Technology Agency, Kawaguchi, Saitama 332-0012, Japan
[3] Institute of Multidisciplinary Research for Advanced Materials, Tohoku University, Sendai 980-8577,
Japan
[4] Department of Physics, Kansas State University, Manhattan, KS 66506-2604, USA

Abstract
Based on the concept of the recently developed quantitative rescattering theory for the
momentum distributions of high-energy photoelectrons generated by infrared lasers, we
applied the theory to extract large-angle elastic differential cross sections (DCS) of the target
ions with free electrons. Using experimental photoelectron spectra for rare gas atoms of Ne,
Ar, Kr and Xe, we showed that the extracted DCS are in good agreement with the DCS
calculated theoretically. The current method of retrieval does not require precise knowledge of
the peak laser intensities. The results show that accurate DCS between electron–ion scattering
indeed can be retrieved from experimental photoelectron spectra generated by lasers, thus
paving the way for using infrared laser pulses for dynamic chemical imaging of transient
molecules with temporal resolution of few femtoseconds.

(Some figures in this article are in colour only in the electronic version)

1. Introduction

Much of our knowledge of the nonlinear interaction of intense laser radiation with atoms and molecules comes from the study of above-threshold ionization (ATI), which is characterized by a sequence of peaks in the electron spectrum, spaced by the photon energy. In recent years femtosecond infrared lasers with peak intensity in the TW to PW cm^{-2} range have become widely available. Together with the introduction of cold-target recoil ion momentum spectroscopy (COLTRIMS) detectors or other advanced electron spectrometers, ATI electrons have been measured over a broad range of energies and angles. Equivalently, these data have been presented as two-dimensional (2D) electron momentum spectra [1, 2]. These experimental data reveal considerable structure not only in the electron energy distributions, but also in the angular

distributions. Most of these studies focus on low energy electrons which are generated either by a multiphoton ionization mechanism or by the tunnelling ionization mechanism. According to the 'conventional' wisdom, depending on the Keldysh parameter, $\gamma = \sqrt{I_p/2U_p}$, where I_p is the ionization energy of the target and U_p the ponderomotive energy, if γ is much larger than 1, the ATI electrons are generated by multiphoton processes, while if γ is much smaller, tunnelling ionization is responsible for producing the low energy electrons. However, such a distinction is by no means clear-cut. In [2], experimentally the 2D electron momentum spectra display pronounced fan-like structures even for laser intensities well into the tunnelling ionization regime. Theoretical studies [3, 4] obtained from the solution to the time-dependent Schrödinger equation (TDSE) in the single active electron approximation show that even in the tunnelling

J. Phys. B: At. Mol. Opt. Phys. **42** (2009) 105205

T Morishita *et al*

region, photoelectron spectra do exhibit features that can be identified with the absorption of integer number of photons. Further studies show that experimental data can be explained quantitatively from TDSE calculations if the contributions of electrons from the whole laser focused volume are included [5].

While low-energy electrons, with energy less than about $2U_p$, account for the majority of electrons generated by an intense laser, already since 1993 photoelectrons extending to $10U_p$ or more have been reported. The energy distributions of these electrons remain nearly constant until a new cut-off at about $10U_p$ is reached. They are known as high-energy plateau photoelectrons. Experiments showed that they exhibit pronounced sidelobes [6–9] extending to large angles with respect to the laser polarization axis. These high-energy ATI electrons have been interpreted using the rescattering model [10]. According to this model, electrons that are freed from the target atom at some well-defined ionization time may be driven back to revisit their parent ion. If these returning electrons are backscattered by the target ion, they can be further accelerated by the laser field and emerge at high energies, reaching up to about $10U_p$. However, the plateau electron spectra, with energies from 4 to $10U_p$, are not always similar for different targets. For xenon atoms, the plateau is rather flat, but for others like krypton or argon atoms, the plateau drops steeply as the electron energy increases. Furthermore, the shape of the plateau is also laser intensity dependent and wavelength dependent. The origin of these differences, while had been allured to the electron–ion elastic scattering cross sections [8], have not been analysed in a quantitative fashion since their initial observations in the 1990s.

Recently, we have re-examined these high-energy photoelectrons theoretically. Based on accurate numerical results obtained from solving the TDSE for atomic targets, we first established the quantitative rescattering (QRS) theory. In the QRS theory, we showed that the 2D high-energy photoelectron momentum spectra can be modelled quantitatively due to the backscattering of the returning electrons by the target ion. The theory was first established theoretically for returning electrons having about the maximum kinetic energy of $3.17U_p$ [11]. It predicts that one can extract elastic differential cross sections (DCS) of target ions with free electrons from the measured high-energy ATI spectra. This prediction was confirmed soon after experiments by Okunishi *et al* [12] and by Ray *et al* [13]. However, these earlier works have limitations. To begin with, the model was established only for electrons which return with the maximum kinetic energy, leaving a large portion of the photoelectron spectra in the rescattering region untouched. Furthermore, in a typical laser experiment, electrons are collected from the whole interaction volume where the laser intensity is not uniform. Thus it is not possible to even assign a single U_p in the experiment without additional assumptions. More recently, in Chen *et al* [14] we have extended the QRS theory to the whole high-energy photoelectrons typically with energy above $4U_p$. In this paper, we used the new extended QRS theory to analyse the experimental data of Ne, Ar and Xe, some of which were first reported in Okunishi *et al* [12],

and some like Kr are first reported here. In section 2 we briefly describe the experimental method and the QRS theory first reported in [14]. In section 3 we show how to extract the DCS from the experimental photoelectron spectra. The results are then compared to theoretically calculated DCS. The last section gives a short summary.

2. Experimental method and the quantitative rescattering theory

The experimental setup is almost the same as that reported previously [15–17]. In brief, we detected electrons using a 264 mm long linear time-of-flight spectrometer with a limited detection angle ($\sim 0.0014 \times 4\pi$ sr). The fundamental output (800 nm) from an amplified Ti:sapphire laser system (pulse width: 100 fs, repetition rate: 1 kHz) was used as the ionizing radiation. The laser beam was focused by an $f = 60$ mm lens to ionize Ne, Ar, Kr and Xe atoms, which are effusively introduced into the vacuum chamber. Typical working pressure within the vacuum chamber is $10^{-6} \sim 10^{-8}$ mb and base pressure is less than 10^{-9} mb. The polarization direction of the laser was varied using a $\lambda/2$ plate. This plate was rotated with a constant speed of exactly one rotation per minute. The total data acquisition time was typically 2–4 h, averaging over several hundred rotations of the electric vector. To obtain peak laser intensity at the ionization point, we measured the ratios of Xe^{2+}/Xe^+ and compared them to the ratios reported by Talebpour *et al* [18]. We also measured photoelectron spectra with circularly polarized light to estimate the peak intensity. However, as will be discussed below, for the purpose of extracting the DCS, no knowledge of the precise laser intensities is needed.

The detailed explanation of the QRS theory has been given recently [19]. Thus only the essentials for the present work will be addressed. According to the QRS theory, high-energy photoelectron momentum distributions, $D(\mathbf{p})$, can be expressed simply as

$$D(\mathbf{p}) = W(p_r)\sigma(p_r, \theta_r), \tag{1}$$

where $\sigma(p_r, \theta_r)$ is the elastic DCS of free electrons, with momentum p_r, by the target ion. Here θ_r is the scattering angle with respect to the direction of the returning electrons along the laser polarization axis. In this equation, $W(p_r)$ is interpreted as the momentum distribution of the returning electrons, to be called returning wave packet in this paper.

In order to use equation (1), the relation between the returning electron momentum $\mathbf{p}_r$ and the photoelectron momentum $\mathbf{p}$ should be established. Let the polarization direction of the linearly polarized laser be along the z-axis. The direction perpendicular to it is to be called the y-axis. For atomic targets, the electron spectra exhibit cylindrical symmetry along the z-axis. In [19], it has been shown that one can write

$$p_z = p\cos\theta = \pm(p_r/1.26 - p_r\cos\theta_r), \tag{2}$$

$$p_y = p\sin\theta = p_r\sin\theta_r, \tag{3}$$

where the '+' and '−' signs in equation (2) refer to electrons that enter towards the ion from the 'right' and the 'left',
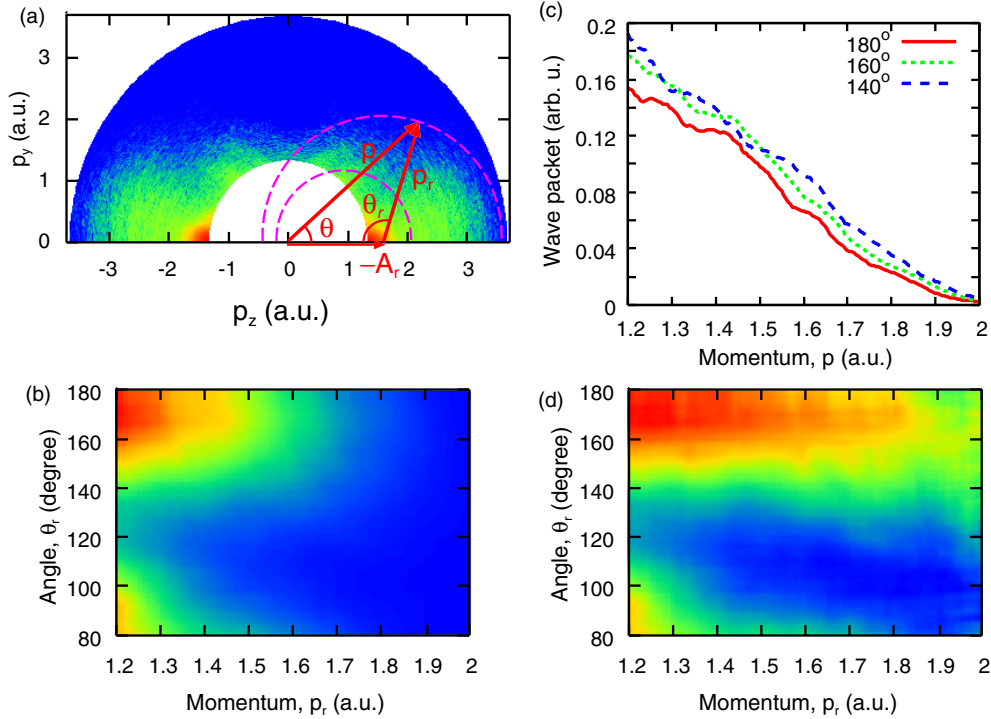
Figure 1. (a) Two-dimensional photoelectron distribution of Ne in a 100 fs laser pulse at the peak intensity of 3.5×10^{14} W cm^{-2}. The image is plotted in the logarithmic scale. (b) High-energy part of the photoelectron distributions between the dotted circles in (a) for large angles as a function of the rescattering electron momentum, (p_r, θ_r) in linear scale. (c) Momentum distribution of the wave packet extracted from experimental data using theoretical elastic differential cross sections. (d) Elastic differential cross sections extracted from experimental data using the momentum distribution of the wave packet at $\theta_r = 160°$.

respectively, and this relation is shown in figure 1(a). Note that $p_r/1.26 = A_r$, where $A_r = A(t_r)$ is the vector potential at the time when the electron returns to the core, at $t = t_r$. Similarly $p_r = p_r(t_r)$ is the electron momentum at the time of return. The relation $p_r/1.26 = A_r$ states that the returning electron momentum is determined by the vector potential at the time of electron return only. This relation would give electrons reaching the maximum kinetic energy of $3.17U_p$ if they return at the time when the vector potential is near the maximum. Further details to justify the relation $p_r = 1.26A_r$ can be found in [19]. Using this relation, the peak laser intensity does not enter equations (2) and (3), thus allows us to decouple the two terms on the right-hand side of equation (1). Note that the term $p_r/1.26 = A_r$ in equation (2) means that an additional momentum $\pm A_r$ will be added to the momentum of the photoelectron along the polarization direction as it exits the laser field. (See figure 1(a).)

Since $\sigma(p_r, \theta_r)$ as well as the relation between $\mathbf{p}_r$ and $\mathbf{p}$ is independent of laser intensity, we can integrate equation (1) over focus volume to obtain

$$S_{I_0}(\mathbf{p}) = \bar{W}_{I_0}(p_r)\sigma(p_r, \theta_r), \qquad (4)$$

where $S_{I_0}(\mathbf{p})$ is the volume-integrated photoelectron momentum distributions from a laser beam which has a peak intensity of I_0 at the laser focus, and $\bar{W}_{I_0}(p_r)$ is the volume-integrated wave packet, namely,

$$\bar{W}_{I_0}(p_r) = \rho \int_0^{I_0} W_I(p_r) \left(-\frac{\partial V}{\partial I}\right) dI \qquad (5)$$

with $W_I(p_r)$ being the wave packet for the laser pulse at a single intensity I and ρ being the density of the target gas. Here, $-\partial V/\partial I\, dI$ represents the volume element for having the intensity between I and $I + dI$. Since $S_{I_0}(\mathbf{p})$ describes the 2D electron momentum distributions measured experimentally, we can use equation (4) to extract the DCS.

3. Extracting elastic electron–ion scattering cross sections from experimental high-energy ATI electron momentum spectra

Equation (4) shows that the experimental 2D electron momentum distributions, $S_{I_0}(\mathbf{p})$, for photoelectrons with momentum p at an angle θ can be expressed as the product of a volume-integrated wave packet, $\bar{W}_{I_0}(p_r)$, and elastic DCS, $\sigma(p_r, \theta_r)$, of the target ion with electrons. If one can calculate $\bar{W}_{I_0}(p_r)$ or obtain it in some other way, then the DCS can be directly extracted from equation (4). In our previous work [14, 19, 20] we showed that $W_I(p_r)$ can be conveniently calculated, if the laser parameters and focusing conditions are given. For the present purpose, we will first show that equation (4) is indeed valid by assuming that we know the DCS, $\sigma(p_r, \theta_r)$, accurately. By choosing a fixed returning electron momentum, (p_r, θ_r), we can calculate the photoelectron momentum, (p, θ), from equations (2) and (3). From equation (4) we can thus calculate $\bar{W}_I(p_r)$, employing theoretical $\sigma(k_r, \theta_r)$.

In figure 1(a), we show the 2D experimental photoelectron spectrum of Ne at the laser intensity of $I_0 = 3.5 \times$
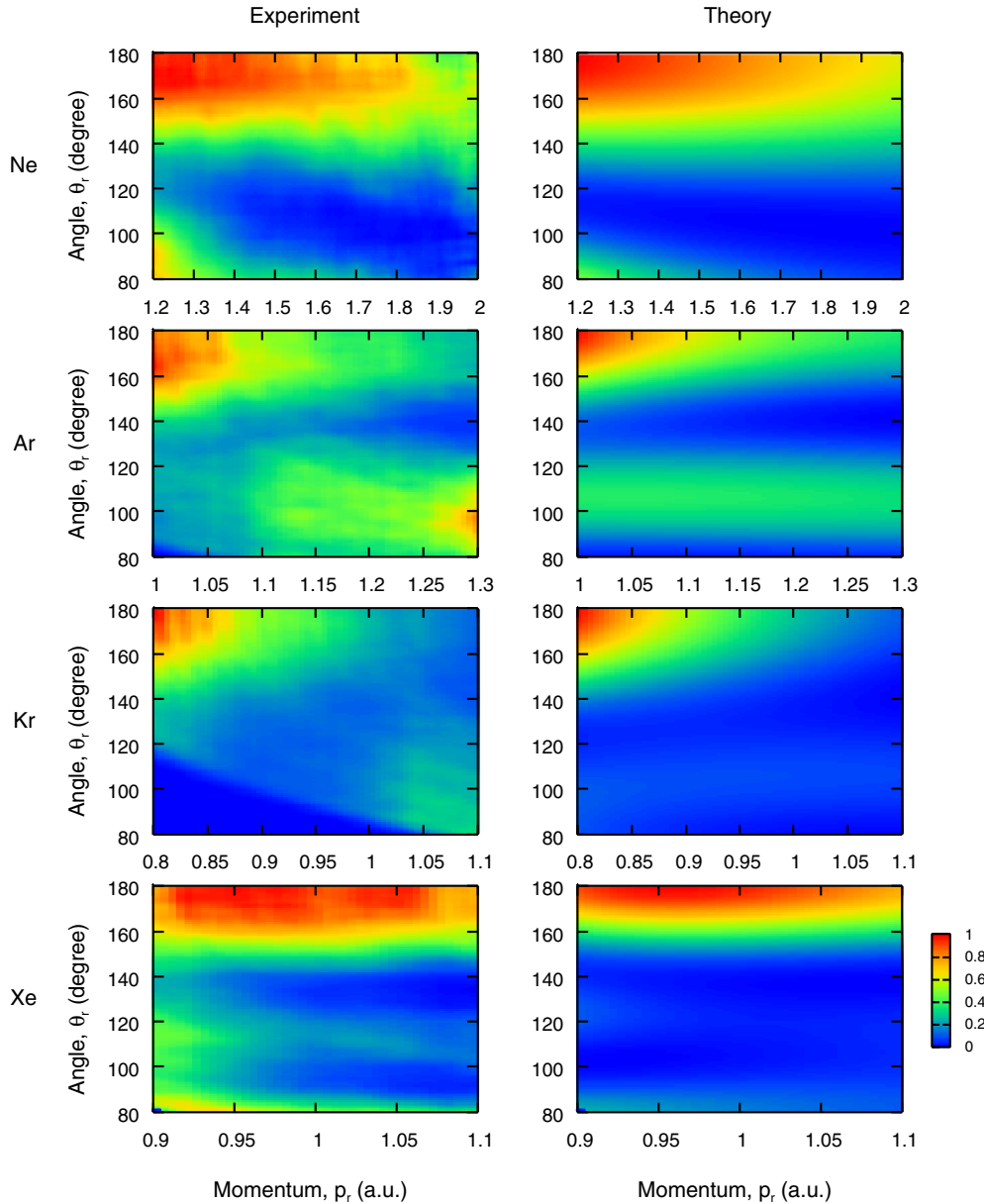
Figure 2. Elastic differential cross sections extracted from experimental data (left) and calculated in the single active electron approximation (right).

10^{14} W cm^{-2}. (The precise intensity of the experiment is not important.) In figure 1(b), we replot the high-energy part of the spectra between the two dashed circles in figure 1(a) as a function of the rescattering electron momentum, (p_r, θ_r). To smooth out the ATI peaks, the electron spectra in figure 1(b) are obtained by integrating over a bin of $\Delta p_r = 0.05$ au and $\Delta \theta_r = 10°$. In figure 1(c), we show the volume-integrated wave packet, $\bar{W}_{I_0}(p_r)$, extracted from the experimental data. We can see that $\bar{W}_I(p_r)$ from $\theta_r = 140°$, $160°$ and $180°$ are nearly on top of each other. Assuming that the wave packet indeed be independent of θ_r, we can use $\bar{W}_{I_0}(p_r)$ from $\theta_r = 160°$ to obtain $\sigma(p_r, \theta_r)$ for all other angles θ_r. The results are shown in figure 1(d).

We applied the same method to extract the DCS from the experimental data for Ar, Kr and Xe. The extracted DCS are shown in the left column of figure 2 together with that from

Ne. On the right-hand column, the differential cross sections calculated theoretically in the single active electron model are shown. The same data are shown at selected electron momentum values, plotted against the scattering angles in figure 3 for easier quantitative comparison. We can see a large degree of agreement between each pair in a broad range of angles and energies, illustrating that the QRS model in the form of equation (4) works very well for experimental data. Looking into more details, the agreement is better in the covered energy region for Ne and Xe. For Ar and Kr, the agreement between the cross sections extracted from the experimental data and from the theory appears to be a little bit larger in the region of large electron momentum and small angles (the lower right quadrant of each frame). This larger error may be due to the small DCS at the scattering angle of 160° for both systems in the higher momentum region, which introduces larger error in
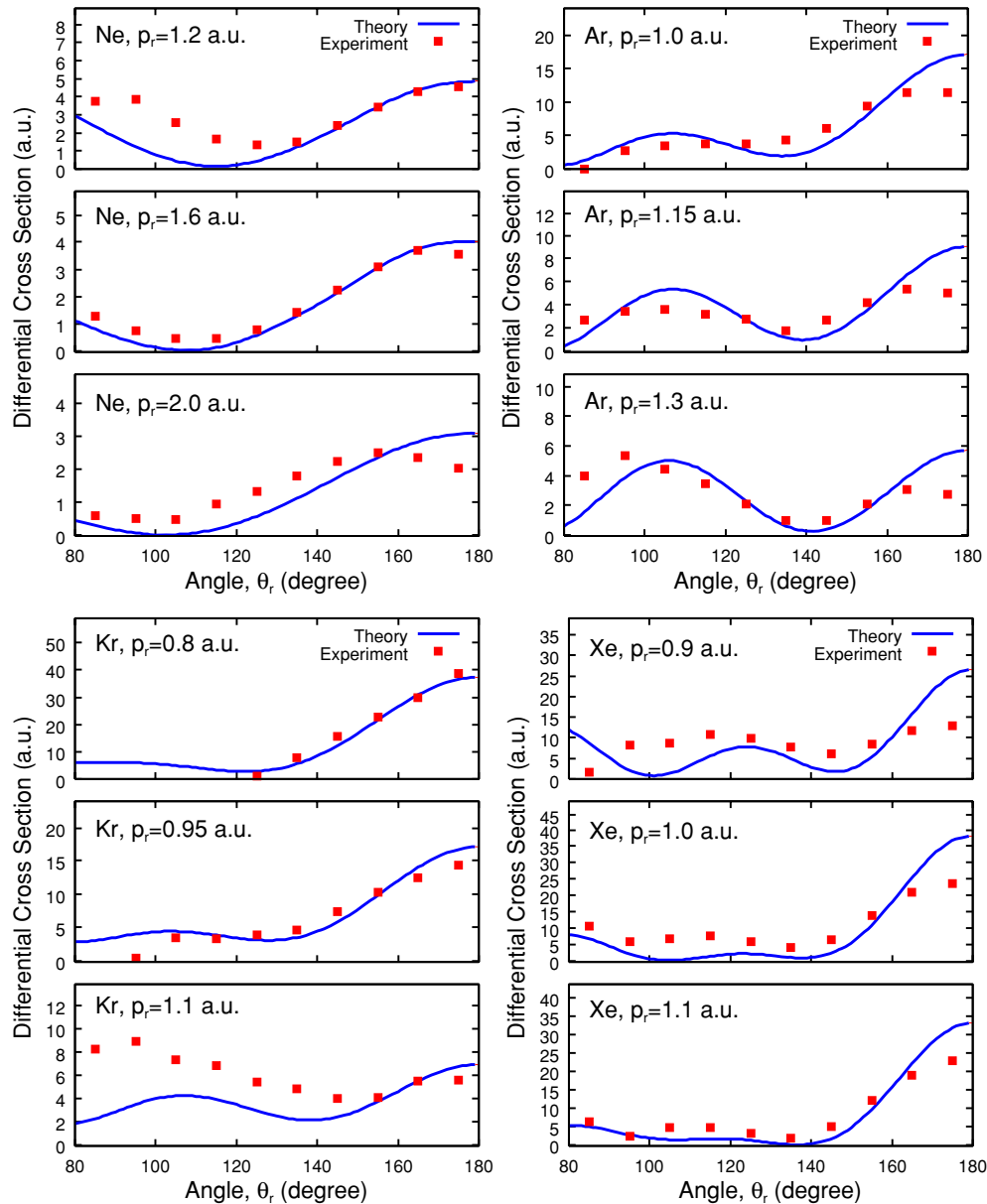
Figure 3. Comparison of theoretical and experimental elastic differential cross sections extracted from photoelectron momentum spectra at selected values of electron momentum. The data are taken from figure 2.

the derived volume-integrated wave packet. Thus we believe that the discrepancy is mostly due to the error introduced by the small signals. With these experimentally extracted DCS over a range of electron energies, they can be used to extract the effective static interaction potential (the potential in the single active electron model) between the incident electron with the target ion. This indicates that one can use laser-induced high-energy ATI spectra to probe the target atom structure.

4. Summary and outlook

In this paper we have successfully extracted the elastic scattering differential cross sections (DCS) of singly charged ions of rare gas atoms by free electrons at large angles from the momentum distributions of high-energy photoelectrons

generated by infrared laser pulses. The essential idea is based on the recently developed quantitative rescattering theory [11, 14, 19], where we have shown that high-energy photoelectron momentum distributions can be expressed as the product of a returning electron wave packet with the DCS for the collision between free electrons and target ions at large angles. (An earlier parametrization has been made in [21] also.) In particular, the theory has been shown to apply to experimental electron spectra where photoelectrons are collected from spatially distributed laser intensities. In the future, it is possible to apply the present method to extract DCS for more complex molecular targets by comparing the photoelectron spectra with the known simple rare gas targets used here under the same laser pulse. When such experiments are carried out in a pump-probe scheme, where a pump laser is used to align the molecule, or to excite the molecule to some

excited states, a probe beam can then be used to generate high-energy photoelectron momentum distributions of the transient molecules. By applying the probe beam also to atomic targets where the DCS are well known, it is possible to extract the change of the DCS for the transient molecules versus the time delay. Since probe pulses with duration of a few femtoseconds are readily available these days, this method can be used for dynamic chemical imaging with temporal resolution of a few femtoseconds. Our results presented in this work shows that the effect of collecting electrons from the whole laser focus volume and the lack of precise knowledge of lasers do not limit this versatile method by comparing the spectra of the unknown system with simple atomic targets. The present results thus serve to illustrate that dynamic chemical imaging of atomic and molecular targets with infrared lasers indeed is possible [22].

Acknowledgments

References

[1] Rudenko A, Zrost K, Schröter C D, de Jesus V L B, Feuerstein B, Moshammer R and Ullrich J 2004 *J. Phys. B: At. Mol. Opt. Phys.* **37** L407
[2] Maharjan C M, Alnaser A S, Litvinyuk I, Ranitovic P and Cocke C L 2006 *J. Phys. B: At. Mol. Opt. Phys.* **39** 1955
[3] Chen Z, Morishita T, Le A-T, Wickenhauser M, Tong X M and Lin C D 2006 *Phys. Rev.* A **74** 053405
[4] Arbó D C, Yoshida S, Persson E, Dimitriou K I and Burgdöorfer J 2006 *Phys. Rev. Lett.* **96** 143003
[5] Morishita T, Chen Z, Watanabe S and Lin C D 2007 *Phys. Rev.* A **75** 023407
[6] Yang B, Schafer K J, Walker B, Kulander K C, Agostini P and DiMauro L F 1993 *Phys. Rev. Lett.* **71** 3770
[7] Grasbon F, Paulus G G, Walther H, Villoresi P, Sansone G, Stagira S, Nisoli M and Silvestri S D 2003 *Phys. Rev. Lett.* **91** 173003
[8] Gaarde M B, Schafer K J, Kulander K C, Sheehy B, Kim D and DiMauro L F 2000 *Phys. Rev. Lett.* **84** 2822
[9] Paulus G G, Nicklich W, Huale Xu, Lambropoulos P and Walther H 1994 *Phys. Rev. Lett.* **72** 2851
[10] Paulus G G, Becker W, Nicklich W and Walther H 1994 *J. Phys. B: At. Mol. Opt. Phys.* **27** L703
[11] Morishita T, Le A-T, Chen Z and Lin C D 2008 *Phys. Rev. Lett.* **100** 013903
[12] Okunishi M, Morishita T, Prümper G, Shimada K, Lin C D, Watanabe S and Ueda K 2008 *Phys. Rev. Lett.* **100** 143001
[13] Ray D *et al* 2008 *Phys. Rev. Lett.* **100** 143002
[14] Chen Z, Le A-T, Morishita T and Lin C D 2009 *J. Phys. B: At. Mol. Opt. Phys.* **42** 061001
[15] Hatamoto T, Okunishi M, Lischke T, Prümper G, Shimada K, Mathur D and Ueda K 2007 *Chem. Phys. Lett.* **439** 296
[16] Mathur D, Hatamoto T, Okunishi M, Prümper G, Lischke T, Shimada K and Ueda K 2007 *J. Phys. Chem.* A **111** 9299
[17] Okunishi M, Shimada K, Prümper G, Mathur D and Ueda K 2007 *J. Chem. Phys.* **127** 064310
[18] Talebpour A, Chien C-Y and Chin S L 1996 *J. Phys. B: At. Mol. Opt. Phys.* **29** L677
[19] Chen Z, Le A-T, Morishita T and Lin C D 2009 *Phys. Rev.* A **79** 033409
[20] Chen Z, Morishita T, Le A-T and Lin C D 2007 *Phys. Rev.* A **76** 043402
[21] Goreslavskii S P and Popruzhenko S V 1999 *J. Phys. B: At. Mol. Opt. Phys.* **32** L531
[22] Morishita T, Le A-T, Chen Z and Lin C D 2008 *New J. Phys.* **10** 025011